Hindawi
International Journal of Intelligent Systems
Volume 2024, Article ID 9199410, 13 pages
https://doi.org/10.1155/2024/9199410

Research Article

Adaptive Threshold Learning in Frequency Domain for Classification of Breast Cancer Histopathological Images

Yujian Liu,[1,2] **Xiaozhang Liu**,[3] **and Yuan Qi**[3]

[1]*School of Information and Communication Engineering, Hainan University, Haikou, China*
[2]*Department of Radiation Oncology, Sun Yat-Sen University First Affiliated Hospital, Guangzhou, China*
[3]*School of Computer Science and Technology, Hainan University, Haikou, China*

Correspondence should be addressed to Xiaozhang Liu; lxzh@hainanu.edu.cn

Received 25 September 2023; Revised 14 February 2024; Accepted 24 February 2024; Published 11 March 2024

Academic Editor: Alexander Hošovský

Breast cancer has become the most common cancer in the world, and biopsy is the most reliable and widely used technique for detecting breast cancer. However, observation of histopathological images is time-consuming and labor-intensive. Currently, CNN has become the mainstream method for breast cancer histopathological image classification research. However, some studies have found that the optical microscope-generated histopathological images have noise, and the output of a well-trained convolutional neural network in image classification tasks can change drastically due to small variations in the input. Therefore, the quality of the image significantly affects the accuracy of the classification. Wavelet transform is a commonly used denoising method, but the selection of the threshold is a difficult problem, and traditional methods are difficult to find the appropriate threshold quickly and accurately. This paper proposes an adaptive threshold selection method that combines threshold selection steps with deep learning methods by using the threshold as a parameter in the CNN model to train. In this way, we associate the threshold with the classification result of the model and find the appropriate value for that image and task by back-propagation in training. The method was experimented on publicly available datasets BreaKHis and BACH. The results in BreaKHis (40x: 94.37%, 100x: 93.85%, 200x: 91.63%, 400x: 93.31%), and BACH (91.25%) demonstrate that our adaptive threshold selection method can improve classification accuracy and is significantly superior to traditional threshold selection methods.

1. Introduction

Cancer is the second leading cause of death globally, and breast cancer has now replaced lung cancer as the most common cancer in the world [1, 2]. Accurate diagnosis of breast cancer is crucial for successful treatment and reducing mortality rates. There are different detection techniques used for diagnosis, such as biopsy, ultrasound (US), magnetic resonance imaging (MRI), and infrared thermography. Among them, biopsy is the most reliable and widely used technique for detecting breast cancer [3]. This requires pathologists to observe the morphology of the tissue under a microscope and make a diagnosis [4]. However, pathologists who can make accurate diagnoses require years of training, and the diagnostic process is time-consuming and laborious [5]. Targeted computer-aided diagnosis systems can help improve the efficiency of breast cancer tissue pathology diagnosis and facilitate the examination of more patients [6].

In recent years, the CNN (convolutional neural network) methods that have demonstrated significant advantages in image classification tasks have been widely applied to medical image classification tasks. Also, it has become the mainstream method for breast cancer histopathology image classification research and has shown significant advantages over traditional methods on publicly available datasets [7–10]. However, some studies have found that the output of a well-trained CNN in image classification tasks can undergo significant variations due to minor variations in the input, and the quality of the image can significantly affect the accuracy of classification [11, 12]. Histopathological images generated by optical microscopes contain noise, which mainly originates from three sources [13–15]:

(1) Uneven or excessively strong lighting from the light source can create reflections or shadows, leading to noise in the image such as glare or black spots.

(2) The instrument itself may also contribute to noise that affects the quality of the image. For example, the optical components of a microscope may have issues such as chromatic aberration or distortion, leading to noise in the image such as color shifts or distortions.

(3) The preparation process of tissue specimens can also have an impact on the quality of the image. For instance, the slicing process may result in uneven thickness, cracks, etc., leading to noise in the image such as discontinuity or blurriness.

Therefore, when classify histopathological images, it is necessary to denoise to ensure the accuracy and reliability of the analysis results.

Wavelet transform [16, 17], Gaussian filtering [18], and other filtering methods [19] are commonly used for image denoising. Among them, the wavelet transform is widely used due to its ability to preserve useful information in the original signal [20, 21]. Threshold selection is an important step in wavelet denoising, as it determines which detail coefficients will be filtered out. However, the commonly employed threshold calculation formulas yield varying thresholds. For instance, the Sqtwolog [22] method tends to opt for higher thresholds, while the Minimax [23] method leans towards selecting lower thresholds. The choice of which formula to use is a difficult problem and often relies on experimentation and expertise.

Previous studies often conducted experiments on simulated signals with added noise. Some researchers would empirically try several different threshold calculation formulas and then use SNR (signal-to-noise ratio) as an evaluation metric to select the formula that yielded the best denoising effect. Some studies did not use threshold calculation formulas but instead directly experimented with a large number of thresholds and selected the one that maximized the SNR of the denoised image. However, comparing the SNR metric requires prior knowledge of both the signal and noise, which is not suitable for real images where noise is not clearly. In addition, in classification tasks, the ultimate evaluation metric is accuracy. However, the decision-making process of the model is like a black box, so accuracy may not necessarily be maximized when SNR is at its highest. Moreover, attempting to apply numerous thresholds directly on real images would consume a significant amount of computational resources due to the high cost of deep learning training.

This paper proposes adaptive wavelet threshold method, which combines the threshold selection step with deep learning methods by treating the threshold as parameters in the CNN model and training it together with the model. This approach can link the threshold to the model's classification results and use back-propagation during training to find the appropriate threshold for the image and task. Experimental results indicate that the thresholds trained in our study outperform those computed using both the Sqtwolog and Minimax formulas.

2. Related Work

2.1. Wavelet Threshold. The wavelet transform, as an effective signal processing technique, has been widely applied in the field of image denoising. In the area of denoising histopathological images, wavelet transform methods have also been extensively researched. For example, in [24], denoising methods including wavelet denoising were tested on pancreatic histopathological images, while in [25], wavelet denoising was applied prior to the classification of breast cancer histopathological images.

Factors affecting the effectiveness of wavelet denoising mainly include the selection of wavelets, threshold selection, threshold function selection, and the number of wavelet transforms. The threshold selection step is crucial to the denoising effect as it determines the range of detail coefficients that will be filtered out. Commonly used threshold selection methods include Sqtwolog, RigrSure, VisuShrink, and Minimax [22, 23]. Minimax and RigrSure are relatively conservative and tend to retain more high-frequency coefficients. The other two methods, Sqtwolog and VisuShrink, especially Sqtwolog, can remove more noise but may also remove useful high-frequency signals.

The choice of threshold selection method is a challenging issue, and previous research often requires experimentation to assess which one is better. For example, [26] simulated a noisy signal and then attempted the four threshold selection methods mentioned above, using SNR (signal-to-noise ratio) metric to evaluate the methods. The authors in [27] conducted a more comprehensive comparison of threshold functions. The authors in [28] not only experimented with existing threshold selection methods but also designed new threshold selection methods and compared them using the SNR metric. In addition to simply comparing threshold selection methods, [29] also designed an iterative search method for experimenting with a large number of thresholds and used the SNR metric to evaluate them. While paper [29] is most similar to our research, there are still significant differences. The authors in [29] conducted experiments using simulated signals with added noise and evaluated the thresholds based on SNR. In contrast, we utilize actual images and optimize thresholds based on loss. In comparison, our threshold selection method can be directly applied to images with uncertain noise, and the selected thresholds are closely related to the specific image and classification task at hand.

2.2. Breast Cancer Classification. CNN is the predominant methodology within the realm of image classification. Due to its exceptional performance, CNN has been extensively utilized in the vast majority of breast cancer histopathological image classification research in recent years, as exemplified by various studies [7, 10, 30–41]. These investigations predominantly employ common methods such as VGG [42], DenseNet [43], Xception [44], and ResNet50 [45]. Among these studies, [7, 32, 38, 41, 46] simply employ transfer learning to optimize common models, and [34] specifically fine-tuning the final two residual blocks after utilizing

transfer learning. On this foundation, some research [10, 33, 39, 40, 46] has utilized ensemble learning methods, integrating the classification results of multiple models to enhance accuracy. In addition, attention mechanisms have been integrated in [10]. Some studies have shifted their focus onto the design of loss functions. For instance, the authors in [31] considered the binary classification of benign and malignant, as well as various subclasses of multiclassification simultaneously, to reduce the likelihood of errors occurring in the benign and malignant categories. Also, the authors in [37] penalize overconfident low-entropy output distributions and adapt the predictions to accommodate uniform distributions, rendering them more applicable to various circumstances. Other studies are more concentrated on clinical issues. Unlike previous research that used public datasets for classification [35], utilizing a dataset gathered independently and incorporating two clinically meaningful categories in recent years: progesterone receptor (PR) status (positive or negative) and HER2 Receptor status (positive or negative).

However, the current breast cancer histopathological image classification research utilized is essentially based on methodologies proposed in the preceding years. In recent years, numerous scholars have persistently endeavored and conducted experiments to enhance the CNN. Consistently, advanced baseline networks with superior performance have been proposed. For example, [47, 48] studied the use of large convolution kernels to expand the receptive field and enhance the extraction of shape information. The authors in [49] researched various data augmentation strategies, the authors in [50] studied various tricks of ResNet and ConvNeXt [51] modified the network architecture of ResNeXt to make it more modern and improve model performance in classification, etc. Among them, ConvNeXt, which was publicly released in 2022, conducted detailed research and surpassed the previous first-place Swin Transformer [52] method on the competition dataset. This paper uses some improvements proposed by ConvNeXt and uses the modified ResNeXt as the baseline in our experiments.

3. Methods

This section is a detailed description of the proposed method. The first part introduces the wavelet denoising algorithm, and the second part introduces the network structure.

3.1. Wavelet Denoising. As shown in the upper part of Figure 1, the wavelet denoising includes three steps. The first step is the discrete wavelet transform (DWT), which can decompose the original image containing noise into four coefficients: CA (approximation coefficient), CV (vertical detail coefficient), CH (horizontal detail coefficient), and CD (diagonal detail coefficient).

The second step is to determine the threshold and then perform denoising on CH, CV, and CD. Since the threshold will affect the image input to the classification model, which in turn affects the model's output and loss function, the selection of the threshold is crucial. By linking the threshold with the loss function, the threshold can be optimized during the training process and gradually approach the threshold with good denoising effect.

The third step is to perform the inverse discrete wavelet transform (IDWT) on CA and the denoised CV, CH, and CD to reconstruct the denoised breast cancer histopathological image. The following is a detailed introduction to DWT, IDWT, and adaptive threshold denoising.

3.1.1. DWT and IDWT. For a one-dimensional input signal x, DWT decomposes it into a set of approximation coefficients a_j and detail coefficients d_j, as shown in the following equations:

$$a_j = \sum_n h_n * x_{j,n}, \tag{1}$$

$$d_j = \sum_n g_n * x_{j,n}, \tag{2}$$

where h and g are the low-pass and high-pass filters of the orthogonal wavelet, $x_{j,n}$ is a discrete sample in the input signal, j is the decomposition level, and n is the displacement.

DWT can be used for recursively decomposing the approximation coefficients of the previous level, and the level of the original signal x is 0, as shown in the following equations:

$$a_0 = x, \tag{3}$$

$$a_j = \sum_n h_n * a_{j-1,n}, \tag{4}$$

$$d_j = \sum_n g_n * a_{j-1,n}. \tag{5}$$

IDWT can reconstruct the approximation and detail coefficients into the original signal, as shown in the following equation:

$$x = \sum_n h_n * a_{j-1,n} + \sum_{j=1}^{J} \sum_n g_n * d_{j,n} * 2^{j-1}, \tag{6}$$

where J is the maximum level, and n is the displacement.

Processing a two-dimensional image is similar to processing a one-dimensional signal; that is, performing DWT and IDWT in the horizontal and vertical directions sequentially, as shown in the following equations:

$$CA_j = \sum_h \sum_v h_h * h_v * a_{j-1,h,v}, \tag{7}$$

$$CV_j = \sum_h \sum_v h_h * g_v * a_{j-1,h,v}, \tag{8}$$

$$CH_j = \sum_h \sum_v g_h * h_v * a_{j-1,h,v}, \tag{9}$$

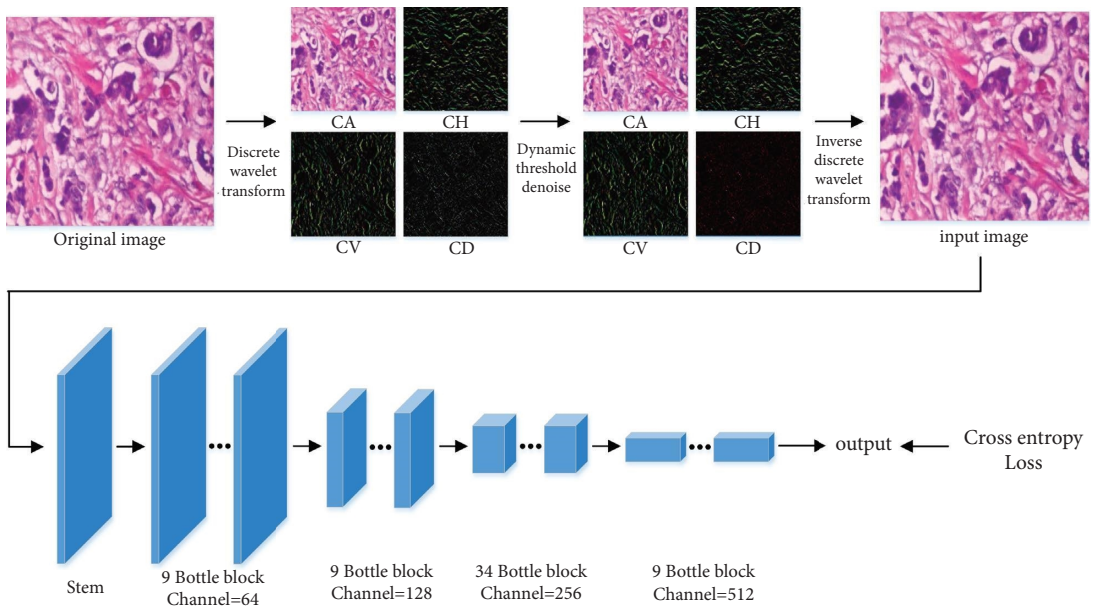

Figure 1: Adaptive wavelet threshold and classification network structure.

$$CD_j = \sum_h \sum_v g_h * g_v * a_{j-1,h,v}, \tag{10}$$

where h and v are horizontal and vertical shifts, respectively. Since the common practice for wavelet denoising is to do DWT and IDWT only once, we focus on the CA, CV, CH, and CD coefficients at level $j = 1$. Higher level coefficients are not experimented in this paper.

3.1.2. Adaptive Threshold Denoising. Firstly, we need to obtain an appropriate threshold through optimization, which is optimized as parameters through back-propagation. Specifically, we initialize a four-dimensional tensor with only one element 1 and input it into a convolutional layer with input channel = 1, output channel = 9, kernel size = 1, stride = 1, and padding = 0. The output channel is set to 9 because the breast histopathological images have three channels of R, G, and B, and each channel's image generates three detail coefficients of CH, CV, and CD after wavelet transform. The nine elements outputted by the convolutional layer are used for denoising the nine coefficients. By this method, changes in the threshold will alter the quality of the image and affect the loss value, and then the threshold will be optimized through back-propagation.

$$\theta^t = \theta^{t-1} - \epsilon_t \frac{\partial L}{\partial \theta}. \tag{11}$$

The method for optimizing parameters is shown as (11), where L is the loss function, ϵ_t is the learning rate, and θ^t is the parameter at the t-th iteration. The learning rate is the most important optimization parameter, as a high learning rate can cause the model to skip the optimal parameters, while a low learning rate can lead to being trapped in local optima. During training, the threshold parameters and classification model parameters are optimized together. However, the range of threshold values (usually a few tens) is much larger than the range of parameter changes in the classification model. Therefore, we set a larger learning rate specifically for the threshold.

After obtaining the threshold, we also need a threshold function to perform denoising. Experimental results have shown that threshold functions with a sudden jump from 0 to 1, such as the commonly used hard thresholding function sgn (), or similar functions that change from 0 to 1 within an extremely small range, perform poorly. In this paper, a sigmoid function is used to construct the threshold function, as shown in the following equation:

$$x_{\text{denoised}} = x_{\text{original}} * \text{sigmoid}\left(\left(x_{\text{original}} - \text{abs}(\text{threshold})\right) * 10\right), \tag{12}$$

where x_{original} is the original detail coefficients, such as CH, CV, and CD, x_{denoised} is the denoised detail coefficients, and threshold is the learned threshold. $x_{\text{original}} - \text{abs}(\text{threshold})$ is used to compare the magnitude of the detail value with the threshold and determine whether the value should be filtered out. Since the optimized parameters may be positive or negative, the abs is used to ensure that the threshold is positive, making it easier to compare with x_{original}.

After applying $x_{\text{original}} - \text{abs}(\text{threshold})$, the values in x_{original} that exceed the threshold become positive, while those below the threshold become negative. Before using sigmoid function, the resulting values are multiplied by 10. Multiplying by 10 allows the function's output to vary from 0.006 to 0.993 within the range of (−0.5 and 0.5) centered around the threshold, resulting in a steeper filter. Using a number that is too large, such as a few hundred, would create a waveform that is too steep and would seriously degrade the threshold's optimization effect. Conversely, using a number that is too small would flatten the waveform

and reduce the filter's effectiveness. Experimental results have shown that 10 is a suitable value.

After using sigmoid function, the output of the threshold function is close to 0 when $x_{\text{original}} - \text{abs}(\text{threshold})$ is less than −0.5 and close to 1 when $x_{\text{original}} - \text{abs}(\text{threshold})$ is greater than −0.5. Assuming threshold is 10, the effect of $\text{sigmoid}((x_{\text{original}} - \text{abs}(\text{threshold})) * 10)$ is shown in Figure 2. Finally, the output of the threshold function is multiplied with x_{original}, where the values in x_{original} that are greater than abs(threshold) are mainly preserved, while the values that are less than abs(threshold) are mostly filtered out.

3.2. Classification Network. The classification network proposed in this paper is shown in the lower part of Figure 1, which has two improvements over the traditional ResNeXt: changing stage compute ratio and fewer activation functions. These improvements refer to the recent exhaustive and thorough findings of ConNeXt. Experiments demonstrate that the improved and more modern ResNeXt performs well in the breast cancer histopathology image classification task in this paper.

3.2.1. Changing Stage Compute Ratio. In the lower part of Figure 1, we employed the ResNeXt-50 structure, whose detailed configuration is presented in Table 1. The "output" column indicates the output dimensions in terms of height (H) and width (W), while the "convolution layers" column describes the shape of the convolution. The first parameter of the convolution layer specifies the size of the convolution kernel, the second parameter denotes the number of channels, and "C = 32" indicates that the convolution is partitioned into 32 groups. The number of residual blocks is specified outside the parentheses. Based on ConvNeXt research, we changed the ratio from the conventional (3, 4, 6) to (3, 9).

3.2.2. Fewer Activation Functions. Block designs for original ResNeXt (left) and improved ResNeXt (right) we used are shown in Figure 3. Compared with the original ResNeXt, we eliminate the ReLU layer below the 1×1 conv. layer in the residual block.

4. Experiment

4.1. Datasets. The BreaKHis and BACH breast cancer histopathological image databases are used in our study. The BreaKHis dataset is the earliest public large-scale non-full-field breast cancer histopathological image dataset. Also, the BACH database is a representative multiclassification dataset.

4.1.1. BreaKHis. BreaKHis was used as an eight-classified dataset, containing four benign tumors: adenosis, fibroadenoma, phyllodes tumor, and tubular adenoma, and four malignant tumors: ductal carcinoma, lobular carcinoma,

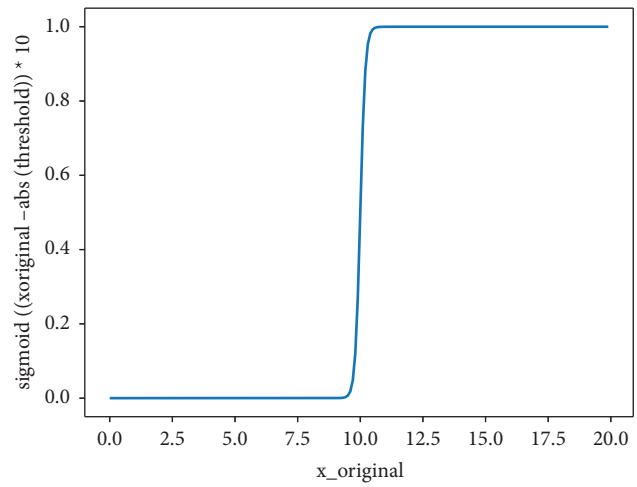

Figure 2: Threshold function.

mucinous carcinoma, and papillary carcinoma. The dataset includes 7909 images collected from 82 patients using four magnification factors (40x, 100x, 200x, and 400x), as shown in Figure 4. The specific image distribution is shown in Table 2. In this dataset, each image has three-channel RGB 8 bit depth in each channel with a resolution of 700x 460 pixels.

4.1.2. BACH. BACH is a four-classified dataset of 400 breast cancer histopathological images, distributed as follows: 100 normal tissue, 100 benign abnormality, 100 in situ carcinoma, and 100 invasive carcinoma. These images are RGB images with 2048×1536 pixels each and a pixel scale of $0.42\,\mu\text{m} \times 0.42$ um, as shown in Figure 4.

4.2. Preprocess. The proposed method was evaluated on BreaKHis dataset and BACH dataset. To reduce the memory and computation overhead, the original images in the BreaKHis dataset were downsampled from 700×460 pixels to 256×256 pixels, and the original images in the BACH dataset were downsampled from 2048×1536 pixels to 512×512 pixels.

To reduce the overfitting caused by the small number of images, we used the data augmentation methods of vertical and horizontal mirroring, random rotations, and random cropping. We also normalize the data.

To evaluate the proposed method, we used k-fold ($k = 4$) cross-validation and divided dataset into four folds, each fold containing 25% of the overall images. During the training process, three sets of data were used for training, while the remaining one set was used for validation. As the proposed method involves searching for suitable thresholds during the training process, the thresholds obtained in each experiment differed slightly. To facilitate comparison with existing threshold selection methods, we first conducted one round of training and validation to obtain a set of thresholds. This set of thresholds was then used for 4-fold cross-validation.

Table 1: Detailed architecture specifications for our ResNeXt-50.

Stage	Output	Convolution layers
Stem	128×128	7×7,64,stride = 2
Res2	64×64	$\begin{bmatrix} 1 \times 1,128 \\ 3 \times 3,128, C = 32 \\ 1 \times 1,256 \end{bmatrix} \times 3$
Res3	32×32	$\begin{bmatrix} 1 \times 1,256 \\ 3 \times 3,256, C = 32 \\ 1 \times 1,512 \end{bmatrix} \times 3$
Res4	16×16	$\begin{bmatrix} 1 \times 1,512 \\ 3 \times 3,512, C = 32 \\ 1 \times 1,1024 \end{bmatrix} \times 9$
Res5	8×8	
#Params		23.0×10^6
FLOPs		5.6×10^9

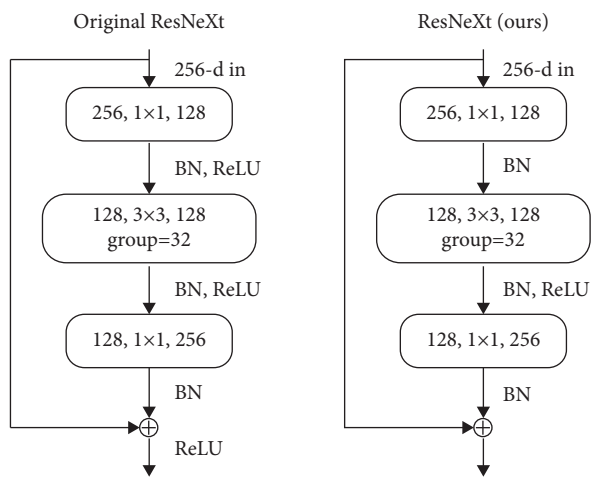

Figure 3: Block designs for original ResNeXt and improved ResNeXt we use.

4.3. Training. The epoch was set to 700 for the BreaKHis dataset, while for the BACH dataset, which has less data, the epoch was set to 2000 to avoid incomplete optimization due to a low number of iterations. As mentioned earlier, the parameters controlling the threshold require a higher learning rate than those in the classification model. For the convolutional layer controlling the threshold, the learning rate used for optimization ranges from a minimum of $2e-3$ to a maximum of $2e-1$. Also, for the convolutional layer in the classification network, the learning rate used for optimization ranges from a minimum of $5e-7$ to a maximum of $5e-5$. The experiments were conducted in the PyTorch environment, using an NVIDIA Titan X GPU.

4.4. Evaluation. In this paper, we use accuracy (ACC) to evaluate the performance of the classification models. As shown in (13), accuracy is the number of examples correctly predicted from the total number of examples.

$$\text{Accuracy} = \frac{T_p + T_n}{T_p + T_n + F_p + F_n}, \tag{13}$$

where T_p and T_n are the true positive and true negative samples, respectively. F_p and F_n are the false positive and false negative samples.

5. Results

We conducted comparative experiments using two representative traditional threshold selection methods: Sqtwolog and Minimax, as shown in (14) and (15), respectively. The Sqtwolog method achieves thorough denoising, but it is also prone to mistaking useful signals for noise and removing them. The Minimax method is more conservative, and it performs better when noise is less distributed in the high-frequency range of the signal.

$$\lambda = \sqrt{2\log(N)}, \tag{14}$$

$$\lambda = \begin{cases} 0.3936 + 0.1829\left(\dfrac{\ln N}{\ln 2}\right), N > 32, \\ 0, N < 32, \end{cases} \tag{15}$$

where N represents the signal length, which in a 2D image refers to the number of pixels. λ is multiplied by the estimated noise variance σ of the image to obtain the threshold used for denoising. The estimated noise variance is shown in the following equation:

$$\sigma = \frac{\text{median}(\text{image})}{0.6745}. \tag{16}$$

In our experiments, we performed threshold denoising on each detail coefficient of the RGB channels separately. Due to the two datasets used and four magnification levels for each dataset, as well as three channels for each image, the number of thresholds used was too numerous to be displayed entirely. As an example, we show the thresholds selected by these two traditional methods and the thresholds

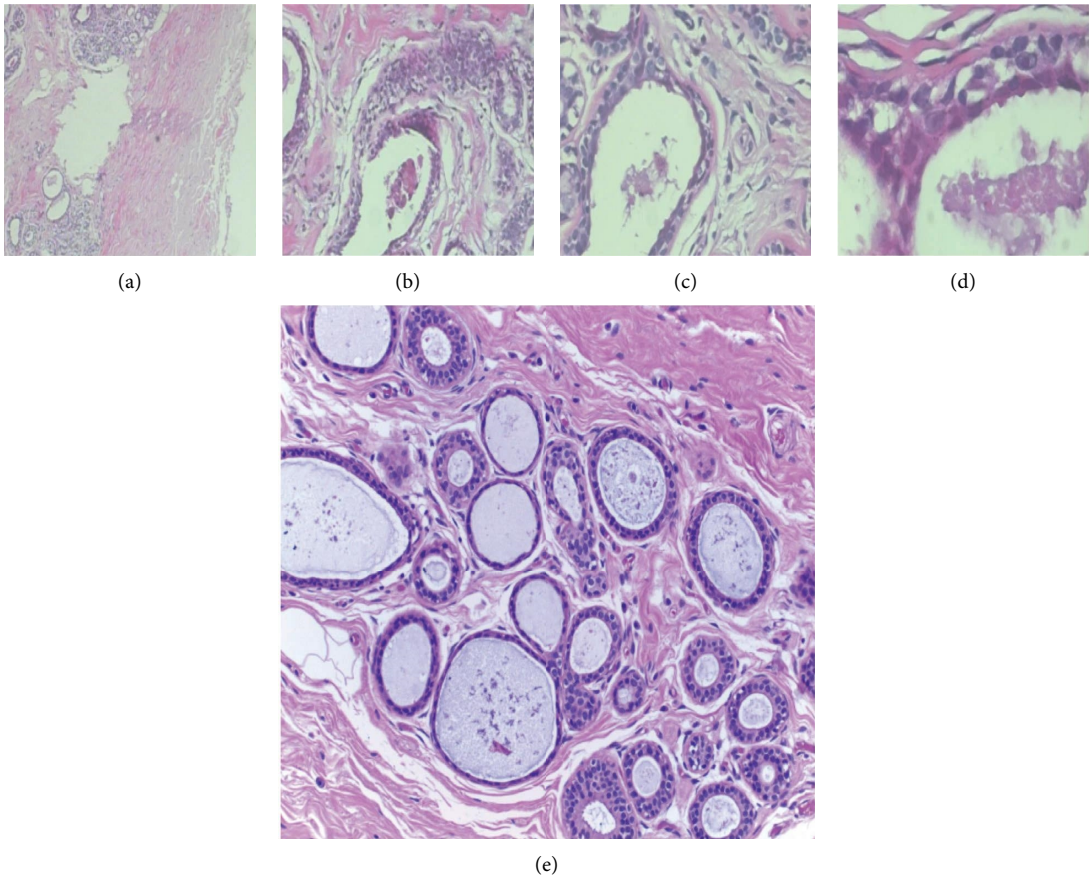

Figure 4: Examples of datasets: (a–d) from BreaKHis and (e) from BACH. (a) 40X. (b) 100X. (c) 200X. (d) 400X. (e) Pixel scale 0.42 μm * 0.42 μm.

Table 2: Image distribution of BreaKHis.

Class	40x	100x	200x	400x
Adenosis	114	113	111	106
Fibroadenoma	253	260	264	237
Phyllodes tumor	109	121	108	115
Tubular adenoma	149	150	140	130
Ductal carcinoma	864	903	896	788
Lobular carcinoma	156	170	163	137
Mucinous carcinoma	205	222	196	169
Papillary carcinoma	145	142	135	138
Total	1995	2081	2013	1820

selected through training by our adaptive method in Table 3, using the 40x images from the BreaKHis dataset.

To validate the effectiveness of our method, we conducted experiments on two datasets: BreaKHis and BACH. The experiments compared the results obtained by using the Sqtwolog method, Minimax method, and our adaptive method for denoising, as well as the results obtained without thresholding denoising processing.

The results in Table 4 show that our adaptive threshold selection method combined with the improved ResNeXt model yields the best results across images at different magnifications. Also, using traditional threshold selection methods, whether it is the larger Sqtwolog or the smaller Minimax, the results obtained are not only inferior to our method but also inferior to the results obtained without performing wavelet threshold denoising. This suggests that the thresholds selected by these methods based on pixel count and median may not be appropriate, resulting in degraded classification results. In contrast, our adaptive method integrates the threshold selection step into deep learning, experiments with a large number of thresholds during training, and continuously adjusts the threshold using the loss function and back-propagation, enabling the selection of more appropriate thresholds. We also compared the results of Inception-v4+SEP and DenseNet121 + SE methods from other papers. The results of these two methods were inferior to those of our method.

In addition, the results of the original ResNeXt and the improved ResNeXt are compared, and it can be seen that the two improvements from the ConNeXt research slightly improved the classification results. We also used the improved ResNeXt as a baseline on the BACH dataset.

Our method not only selects appropriate thresholds but also does so efficiently. Traditional methods often require trying multiple thresholds and selecting the appropriate one based on results. Due to the sensitivity of deep learning models to input changes, comparing the effect of different thresholds on classification results on a well-trained model is

Table 3: Thresholds selection by using different methods.

Method	Channel	CH	CV	CD
Sqtwolog	R	39.19	55.52	39.19
	G	39.19	55.52	39.19
	B	35.92	55.25	35.92
Minimax	R	26.28	37.23	26.28
	G	26.28	37.23	26.28
	B	24.09	35.04	24.09
Adaptive	R	3.13	7.49	12.01
	G	3.60	1.65	14.36
	B	2.54	3.01	7.61

Table 4: Results in BreaKHis dataset.

Method	Accuracy			
	40	100	200	400
Inception-v4 + SEP [53]	85.7 ± 1.9	84.2 ± 3.2	84.9 ± 2.2	80.1 ± 4.4
DenseNet121 + SE [54]	89.1 ± 3.6	85.0 ± 5.1	87.0 ± 6.0	84.5 ± 3.6
Original ResNeXt	94.06 ± 0.44	93.55 ± 0.54	90.73 ± 0.49	92.58 ± 0.26
Improved ResNeXt	94.23 ± 0.39	93.51 ± 0.42	90.84 ± 0.62	92.74 ± 0.17
Improved ResNeXt + Sqtwolog	93.64 ± 0.18	92.86 ± 0.38	90.81 ± 0.33	91.02 ± 0.30
Improved ResNeXt + Minimax	93.72 ± 0.58	92.30 ± 0.63	90.89 ± 0.63	91.84 ± 0.21
Improved ResNeXt + adaptive (ours)	94.37 ± 0.56	93.85 ± 0.38	91.63 ± 0.14	93.31 ± 0.37

unreasonable, as input changes can lead to worse results. Threshold filtering on input images during training can compare the actual effects of different thresholds. However, it is difficult for humans to judge which threshold is better during training and make adjustments. Often the comparison can only be made after the training is completed, which consumes a lot of resources and time. Our method can continuously experiment and adjust thresholds during training, requiring only a few training times to find the appropriate threshold.

Table 5 shows the results of different methods on the BACH dataset. Similar to the results on BreaKHis, our adaptive method performs the best, while the Sqtwolog and the Minimax methods still perform worse than no denoising. Additionally, the variance of the results using our adaptive method and the Minimax method is relatively large. This may be due to the fact that the BACH dataset has much less data than the BreaKHis dataset, resulting in more unstable results. We also compared the results of AHoNet and DenseNet121 + SE methods from other papers. The results of these two methods were inferior to those of our method.

Table 5: Results in BACH dataset.

Method	Accuracy
AHoNet [55]	0.85
Guided soft attention [56]	90.25 ± 1.84
ResNeXt	90.50 ± 0.56
ResNeXt + Sqtwolog	90.25 ± 0.22
ResNeXt + Minimax	88.75 ± 0.89
ResNeXt + adaptive (ours)	91.25 ± 1.12

6. Analysis

To observe the changes of the adaptive wavelet threshold during training, we conducted an experiment using 40x images from the BreaKHis dataset. We recorded the threshold at the end of each epoch and plotted the threshold change curve in Figure 5, Figure 6, and Figure 7. As shown in Table 3, the threshold selected by the Minimax method were mostly around 20, with the maximum being 37.23. It can be seen that the range of adaptive wavelet threshold changes during training was approximately 0 to 35, which covered the values of the Minimax method. This indicates that our adaptive method can generate thresholds similar to those of the Minimax method during training and has tried to do so. Therefore, the reason why the threshold selected by our adaptive method is smaller than that of the Minimax method is that the threshold was optimized to a smaller value during training, rather than due to the setting of parameters related to the training that prevent the threshold close to those selected by the Minimax method.

The range of thresholds selected by the Sqtwolog method is from 35.92 to 55.52, which is not too far from the range of threshold in this experiment. However, the accuracy obtained by this method is inferior to that of the Minimax method and the adaptive method. Therefore, we speculate that the larger threshold selected by the Sqtwolog method is less suitable, and the fact that the threshold selection by adaptive method did not reach 55.52 or even larger values during training is the result of effective optimization.

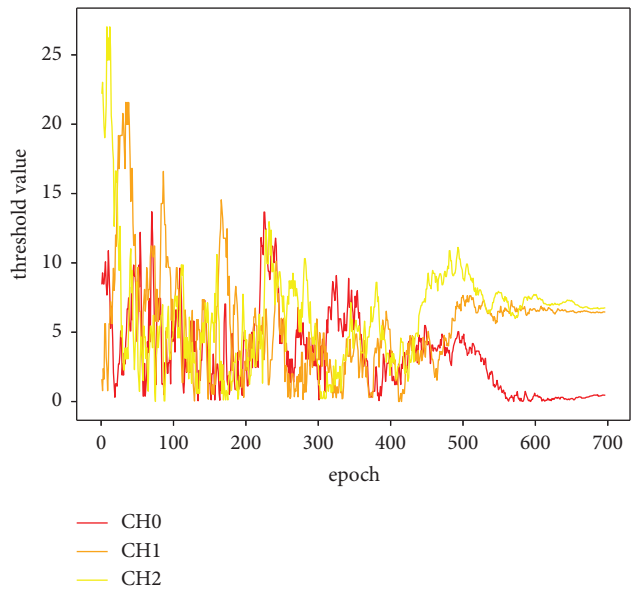

Figure 5: Curve of CH coefficients in training.

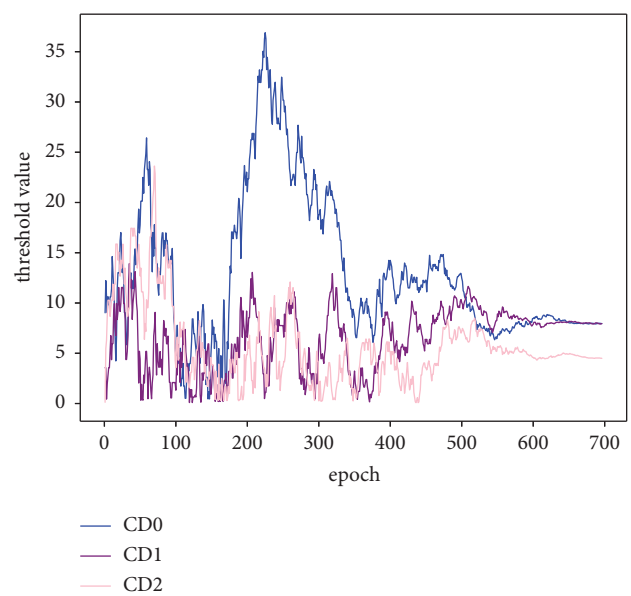

Figure 6: Curve of CD coefficients in training.

7. Visualization

To verify the effectiveness of our adaptive threshold method, we compared the effects of thresholds selection different methods on images, as shown in Figure 8. The selected images were from the validation set of the BreaKHis dataset with a magnification of 40x. The first row shows the original images. The second, fourth, and sixth rows show the images after denoising using different thresholds. The third, fifth, and seventh rows show the differences between the denoised images and the original images. To facilitate observation, we normalized these difference images.

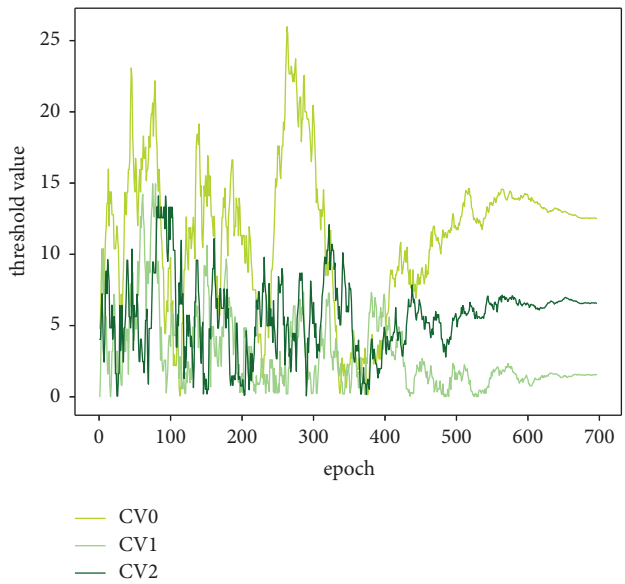

Figure 7: Curve of CV coefficients in training.

For the images in the first and second columns, the difference images show that the threshold selected by the Sqtwolog method has removed many boundaries and texture information. This is also evident in the denoised images, where the boundaries of the tissue are noticeably blurred. The threshold selected by the Minimax method also causes similar problems, but to a lesser extent. This is because the threshold selected by the Minimax method is smaller. Our adaptive method does not have this issue. There are no obvious boundaries or texture information in the difference images, and the denoised images still display this information clearly. This indicates that compared to traditional methods, our adaptive method can effectively preserve useful information.

Because in areas with a large number of cells, it is difficult to distinguish which information is noise. To observe the denoising effect of different threshold selection methods, we selected an image with large blank area as an example, as shown in the third column. After confirmation by a doctor, the light-colored spots in the red box in original image are noise. The white spots in the red box in the difference images indicate that all three thresholds have a denoising effect on these noises. For further analysis, we examined the pixel values in the red box in the difference images.

Taking the maximum value of the pixels in the upper right red box of the difference image as an example, the maximum values corresponding to the Sqtwolog method, Minimax method, and our the adaptive method are 168, 190, and 204, respectively. This roughly indicates that the noise removed by adaptive threshold accounts for a higher percentage of all removed information. This validates the advantage of the adaptive method in Table 4.

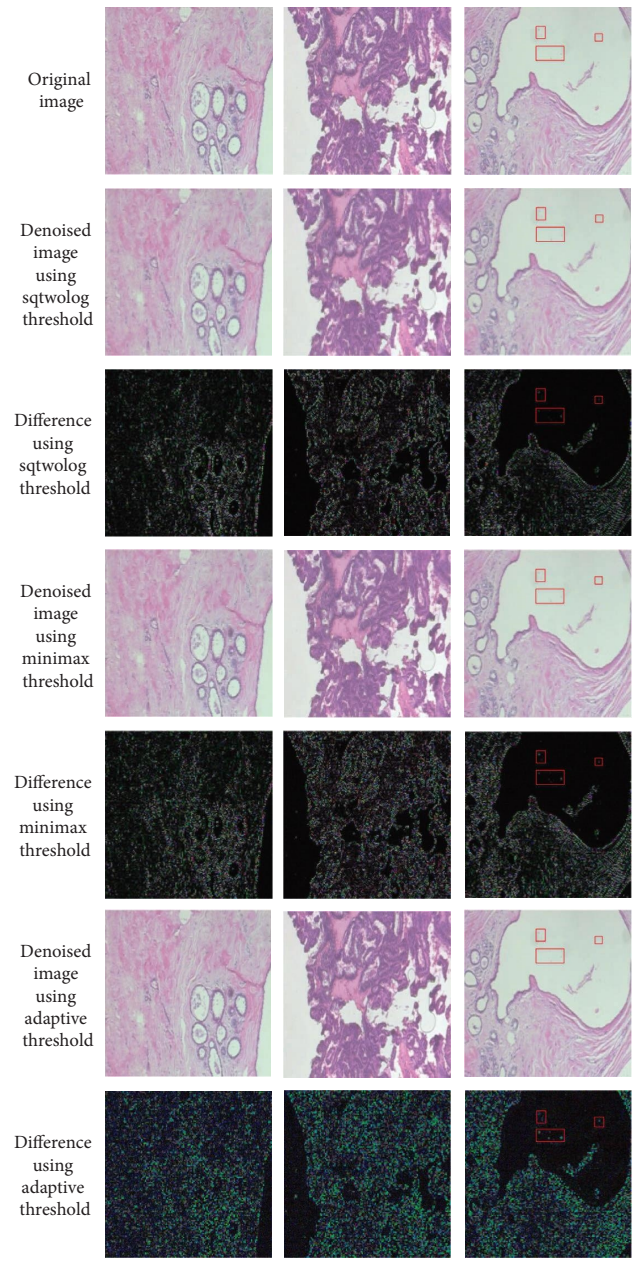

Figure 8: Original images, denoised images, and difference images from BreaKHis dataset.

8. Conclusion

In this study, we propose an adaptive threshold selection method that combines the optimization process of deep learning with wavelet denoising threshold selection. This method establishes a forward and backward propagation between the threshold and the classification loss, allowing for the optimization of the threshold during training. Compared to traditional thresholding methods, this method

can efficiently select appropriate thresholds that balance noise removal and information preservation, leading to higher accuracy of the classification model.

We conducted experiments on the BreaKHis dataset and the BACH dataset, and compared our adaptive method with representative traditional thresholding methods: the Sqtwolog method which tends to produce higher threshold, and the Minimax method which tends to produce lower threshold. The results showed that our adaptive method outperformed the Sqtwolog and Minimax methods and also achieved improved accuracy compared to using the original images.

In addition, we speculate that our adaptive threshold selection method is not only applicable to breast cancer histopathological images but also to other images with noise that are difficult to determine threshold values due to unknown noise frequency or unclear boundary between noise frequency and useful information frequency.

Our research also encounters certain limitations and challenges. This study proposes a method to derive thresholds through training, yet the selection of wavelets is another formidable issue, demanding both expertise and experimentation. The Haar wavelet and the db2 wavelet are commonly employed in the domain of wavelet denoising. Throughout our experiments, we not only delved into the application of the Haar wavelet but also explored the intricacies of the db2 wavelet. Unfortunately, the utilization of the db2 wavelet resulted in a deterioration of outcomes. Should it be possible to assimilate parameters associated with wavelet design into the model for training, perhaps the model could adeptly learn the optimal wavelet for a given image and task. This poses a formidable challenge for us and sets the course for future research endeavors.

Data Availability

The data used in this study are available at BACH dataset at https://iciar2018-challenge.grand-challenge.org/Dataset/ and BreaKHis dataset at https://web.inf.ufpr.br/vri/databases/breast-cancer-histopathological-database-breakhis/.

Conflicts of Interest

The authors declare that they have no conflicts of interest.

Acknowledgments

This work was supported by the Hainan Province Science and Technology Special Fund (Grant no. ZDYF2022GXJS011).

References

[1] N. Pasha and N. C. Turner, "Understanding and overcoming tumor heterogeneity in metastatic breast cancer treatment," *Nature Canada*, vol. 2, no. 7, pp. 680–692, 2021.

[2] C. Hu, S. N. Hart, R. Gnanaolivu et al., "A population-based study of genes previously implicated in breast cancer," *New England Journal of Medicine*, vol. 384, no. 5, pp. 440–451, 2021.

[3] V. Kumar, A. K. Abbas, and J. C. Aster, *Robbins Basic Pathology E-Book*, Elsevier Health Sciences, Amsterdam, The Netherlands, 2017.

[4] A. Binder, M. Bockmayr, M. Hägele et al., "Morphological and molecular breast cancer profiling through explainable machine learning," *Nature Machine Intelligence*, vol. 3, no. 4, pp. 355–366, 2021.

[5] M. Veta, J. P. W. Pluim, P. J. Van Diest, and M. A. Viergever, "Breast cancer histopathology image analysis: a review," *IEEE Transactions on Biomedical Engineering*, vol. 61, no. 5, pp. 1400–1411, 2014.

[6] J. Bai, R. Posner, T. Wang, C. Yang, and S. Nabavi, "Applying deep learning in digital breast tomosynthesis for automatic breast cancer detection: a review," *Medical Image Analysis*, vol. 71, 2021.

[7] N. Ahmad, S. Asghar, and S. A. Gillani, "Transfer learning-assisted multi-resolution breast cancer histopathological images classification," *The Visual Computer*, vol. 38, no. 8, pp. 2751–2770, 2022.

[8] S. Sharma and S. Kumar, "The xception model: a potential feature extractor in breast cancer histology images classification," *ICT Express*, vol. 8, no. 1, pp. 101–108, 2022.

[9] S. Chattopadhyay, A. Dey, P. K. Singh, and R. Sarkar, "Drdanet: dense residual dual-shuffle attention network for breast cancer classification using histopathological images," *Computers in Biology and Medicine*, vol. 145, 2022.

[10] R. Karthik, R. Menaka, and M. V. Siddharth, "Classification of breast cancer from histopathology images using an ensemble of deep multiscale networks," *Biocybernetics and Biomedical Engineering*, vol. 42, no. 3, pp. 963–976, 2022.

[11] R. Geirhos, P. Rubisch, C. Michaelis, M. Bethge, F. A. Wichmann, and W. Brendel, "Imagenet-trained cnns are biased towards texture; increasing shape bias improves accuracy and robustness," 2018, https://arxiv.org/abs/1811.12231.

[12] C. Xie, Y. Wu, L. van der Maaten, A. L. Yuille, and K. He, "Feature denoising for improving adversarial robustness," in *Proceedings of the IEEE/CVF conference on computer vision and pattern recognition*, pp. 501–509, Long Beach, CA, USA, June 2019.

[13] R. Sharma, K. Sharma, and M. Bala, "Analysis of histopathological images: an overview," in *Proceedings of the 2022 International Conference on Computing, Communication, Security and Intelligent Systems (IC3SIS)*, IEEE, Ernakulam, Kerala, India, July 2022.

[14] T. R. Chanu, T. R. Singh, and K. M. Singh, "A new algorithm for removing salt and pepper noise from color medical images," *Multimedia Tools and Applications*, vol. 82, no. 16, pp. 24991–25013, 2023.

[15] M. Tariq, S. Iqbal, H. Ayesha, I. Abbas, K. T. Ahmad, and M. F. K. Niazi, "Medical image based breast cancer diagnosis: state of the art and future directions," *Expert Systems with Applications*, vol. 167, 2021.

[16] Z. Zhang, Y. Lu, C. Lv, Q. Mao, S. Wang, and S. Yan, "Restoration of integrated circuit terahertz image based on wavelet denoising technique and the point spread function model," *Optics and Lasers in Engineering*, vol. 138, 2021.

[17] C. Tian, M. Zheng, W. Zuo, B. Zhang, Y. Zhang, and D. Zhang, "Multi-stage image denoising with the wavelet transform," *Pattern Recognition*, vol. 134, 2023.

[18] Z. Chen, Z. Zhou, and S. Adnan, "Joint low-rank prior and difference of Gaussian filter for magnetic resonance image denoising," *Medical, & Biological Engineering & Computing*, vol. 59, no. 3, pp. 607–620, 2021.

[19] A. Kumar and S. Singh Sodhi, "Comparative analysis of Gaussian filter, median filter and denoise autoenocoder," in *Proceedings of the 2020 7th International Conference on Computing for Sustainable Global Development (INDIACom)*, IEEE, New Delhi, India, March 2020.

[20] J. Gu, T. S. Yang, J. C. Ye, and D. H. Yang, "Cyclegan denoising of extreme low-dose cardiac ct using wavelet-assisted noise disentanglement," *Medical Image Analysis*, vol. 74, 2021.

[21] B. Mishra, "A survey on denoising techniques of ppg signal," in *Proceedings of the 2020 IEEE international conference for innovation in technology (INOCON)*, IEEE, Bangluru, India, November 2020.

[22] P. Kumar and D. Agnihotri, "Biosignal denoising via wavelet thresholds," *IETE Journal of Research*, vol. 56, no. 3, pp. 132–138, 2010.

[23] D. Valencia, D. Orejuela, J. Salazar, and J. Valencia, "Comparison analysis between rigrsure, sqtwolog, heursure and minimaxi techniques using hard and soft thresholding methods," in *Proceedings of the 2016 XXI Symposium on Signal Processing, Images and Artificial Vision (STSIVA)*, IEEE, Bucaramanga, Colombia, August 2016.

[24] M. K. Raczkowska, P. Koziol, S. Urbaniak-Wasik, C. Paluszkiewicz, W. M. Kwiatek, and T. P. Wrobel, "Influence of denoising on classification results in the context of hyperspectral data: high definition ft-ir imaging," *Analytica Chimica Acta*, vol. 1085, pp. 39–47, 2019.

[25] E. Cengiz, M. M. Kelek, Y. Oğuz, and C. Yılmaz, "Classification of breast cancer with deep learning from noisy images using wavelet transform," *Biomedical Engineering/Biomedizinische Technik*, vol. 67, no. 2, pp. 143–150, 2022.

[26] K. Yu, L. Feng, Y. Chen et al., "Accurate wavelet thresholding method for ecg signals," *Computers in Biology and Medicine*, vol. 169, 2024.

[27] A. Halidou and Y. Mohamadou, *Review of Wavelet Denoising Algorithms*, Multimedia Tools and Applications, 2023.

[28] L. Jing-yi, L. Hong, Y. Dong, Z. Yan-sheng et al., "A new wavelet threshold function and denoising application," *Mathematical Problems in Engineering*, vol. 2016, pp. 1–8, 2016.

[29] F. M. Bayer, A. J. Kozakevicius, and R. J. Cintra, "An iterative wavelet threshold for signal denoising," *Signal Processing*, vol. 162, pp. 10–20, 2019.

[30] R. Krithiga and P. Geetha, "Breast cancer detection, segmentation and classification on histopathology images analysis: a systematic review," *Archives of Computational Methods in Engineering*, vol. 28, no. 4, pp. 2607–2619, 2021.

[31] S. Alkassar, B. A. Jebur, M. A. M. Abdullah, J. H. Al-Khalidy, and J. A. Chambers, "Going deeper: magnification-invariant approach for breast cancer classification using histopathological images," *IET Computer Vision*, vol. 15, no. 2, pp. 151–164, 2021.

[32] E. T. Zewdie, A. W. Tessema, and G. L. Simegn, "Classification of breast cancer types, sub-types and grade from histopathological images using deep learning technique," *Health Technology*, vol. 11, no. 6, pp. 1277–1290, 2021.

[33] Y. Zheng, C. Li, X. Zhou et al., "Application of transfer learning and ensemble learning in image-level classification for breast histopathology," *Intelligent Medicine*, vol. 3, no. 2, pp. 115–128, 2023.

[34] S. Boumaraf, X. Liu, Z. Zheng, X. Ma, and C. Ferkous, "A new transfer learning based approach to magnification dependent and independent classification of breast cancer in histopathological images," *Biomedical Signal Processing and Control*, vol. 63, 2021.

[35] Y. Ektefaie, W. Yuan, D. A. Dillon et al., "Integrative multiomics-histopathology analysis for breast cancer classification," *NPJ Breast Cancer*, vol. 7, no. 1, p. 147, 2021.

[36] M. Liu, L. Hu, Y. Tang et al., "A deep learning method for breast cancer classification in the pathology images," *IEEE Journal of Biomedical and Health Informatics*, vol. 26, no. 10, pp. 5025–5032, 2022.

[37] S. Singh and R. Kumar, "Breast cancer detection from histopathology images with deep inception and residual blocks," *Multimedia Tools and Applications*, vol. 81, no. 4, pp. 5849–5865, 2022.

[38] H. Zerouaoui and A. Idri, "Deep hybrid architectures for binary classification of medical breast cancer images," *Biomedical Signal Processing and Control*, vol. 71, 2022.

[39] Y. Wang, B. Acs, S. Robertson et al., "Improved breast cancer histological grading using deep learning," *Annals of Oncology*, vol. 33, no. 1, pp. 89–98, 2022.

[40] M. R. Abbasniya, S. A. Sheikholeslamzadeh, H. Nasiri, and S. Emami, "Classification of breast tumors based on histopathology images using deep features and ensemble of gradient boosting methods," *Computers & Electrical Engineering*, vol. 103, 2022.

[41] S. Kumar and S. Sharma, "Sub-classification of invasive and non-invasive cancer from magnification independent histopathological images using hybrid neural networks," *Evolutionary Intelligence*, vol. 15, no. 3, pp. 1531–1543, 2022.

[42] K. Simonyan and A. Zisserman, "Very deep convolutional networks for large-scale image recognition," 2014, https://arxiv.org/abs/1409.1556.

[43] G. Huang, Z. Liu, L. Van Der Maaten, and K. Q. Weinberger, "Densely connected convolutional networks," in *Proceedings of the IEEE conference on computer vision and pattern recognition*, pp. 4700–4708, Las Vegas, NV, USA, June 2017.

[44] F. Chollet, "Xception: deep learning with depthwise separable convolutions," in *Proceedings of the IEEE conference on computer vision and pattern recognition*, pp. 1251–1258, Honolulu, HI, USA, July 2017.

[45] K. He, X. Zhang, S. Ren, and J. Sun, "Deep residual learning for image recognition," in *Proceedings of the IEEE conference on computer vision and pattern recognition*, pp. 770–778, Las Vegas, NV, USA, June 2016.

[46] D. S. Luz, T. J. B. Lima, R. R. Silva, D. M. V. Magalhães, and F. H. D. Araujo, "Automatic detection metastasis in breast histopathological images based on ensemble learning and color adjustment," *Biomedical Signal Processing and Control*, vol. 75, 2022.

[47] X. Ding, X. Zhang, J. Han, and G. Ding, "Scaling up your kernels to 31x31: revisiting large kernel design in cnns," in *Proceedings of the IEEE/CVF Conference on Computer Vision and Pattern Recognition*, New Orleans, LA, USA, June 2022.

[48] S. Liu, T. Chen, X. Chen et al., "More convnets in the 2020s: scaling up kernels beyond 51x51 using sparsity," 2022, https://arxiv.org/abs/2207.03620.

[49] S. G. Müller and F. Hutter, "Trivialaugment: tuning-free yet state-of-the-art data augmentation," in *Proceedings of the IEEE/CVF international conference on computer vision*, Montreal, BC, Canada, October 2021.

[50] W. Ross, H. Touvron, and H. Jégou, "Resnet strikes back: an improved training procedure in timm," 2021, https://arxiv.org/abs/2110.00476.

[51] Z. Liu, H. Mao, C.-Y. Wu, C. Feichtenhofer, Trevor Darrell, and S. Xie, "A convnet for the 2020s," in *Proceedings of the IEEE/CVF Conference on Computer Vision and Pattern Recognition*, New Orleans, LA, USA, June 2022.

[52] Z. Liu, Y. Lin, Y. Cao et al., "Swin transformer: hierarchical vision transformer using shifted windows," in *Proceedings of the IEEE/CVF international conference on computer vision*, Montreal, BC, Canada, October 2021.

[53] C. Zhu, F. Song, Y. Wang, H. Dong, Y. Guo, and J. Liu, "Breast cancer histopathology image classification through assembling multiple compact cnns," *BMC Medical Informatics and Decision Making*, vol. 19, no. 198, pp. 1–17, 2019.

[54] X. Li, X. Shen, Y. Zhou, X. Wang, and T.-Q. Li, "Classification of breast cancer histopathological images using interleaved densenet with senet (idsnet)," *PLoS One*, vol. 15, no. 5, 2020.

[55] Y. Zou, J. Zhang, S. Huang, and B. Liu, "Breast cancer histopathological image classification using attention high-order deep network," *International Journal of Imaging Systems and Technology*, vol. 32, no. 1, pp. 266–279, 2022.

[56] H. Yang, J.-Y. Kim, H. Kim, and S. P. Adhikari, "Guided soft attention network for classification of breast cancer histopathology images," *IEEE Transactions on Medical Imaging*, vol. 39, no. 5, pp. 1306–1315, 2020.